Classification: Physical Sciences (Chemistry) and Biological Sciences (Cell Biology)

A cell nanoinjector based on carbon nanotubes

Xing Chen[*||], Andras Kis[†||], A. Zettl[†||**], and Carolyn R. Bertozzi[*‡§¶||**]

Departments of [*]Chemistry, [†]Physics and [‡]Molecular and Cell Biology, and [§]Howard Hughes Medical Institute, University of California, Berkeley and [¶]Molecular Foundry and [||]Materials Sciences Division, Lawrence Berkeley National Laboratory, Berkeley, CA 94720

[**]To whom correspondence should be addressed:

Carolyn Bertozzi: crb@berkeley.edu or A. Zettl, e-mail: azettl@berkeley.edu

Abbreviations: CNT, carbon nanotube; MWNT, multi-walled carbon nanotube; AFM, atomic force microscope; SEM, scanning electron microscope; TEM, transmission electron microscope;

Technologies for introducing molecules into living cells are vital for probing the physical properties and biochemical interactions that govern the cell's behavior. Here we report the development of a nanoscale cell injection system—termed the nanoinjector—that uses carbon nanotubes to deliver cargo into cells. A single muti-walled carbon nanotube attached to an atomic force microscope tip was functionalized with cargo via a disulfide-based linker. Penetration of cell membranes with this "nanoneedle", followed by reductive cleavage of the disulfide bonds within the cell's interior, resulted in the release of cargo inside the cells. The capability of the nanoinjector was demonstrated by injection of protein-coated quantum dots into live human cells. Single-particle tracking was employed to characterize the diffusion dynamics of injected quantum dots in the cytosol. This new technique causes no discernible membrane or cell damage, and can deliver a discrete number of molecules to the cell's interior without the requirement of a carrier solvent.

Technologies for introducing exogenous materials into cells play a central role in experimental cell biology. The major challenge is to overcome the barrier imposed by the plasma membrane. This has been accomplished in a variety of ways, such as permeabilization of the membrane with lipids, electric currents, or pore-forming toxins, and physical penetration with a micropipette (i.e., microinjection) or microprojectile (1). Each method has its advantages and disadvantages, but one common liability is physical damage to the cell membrane.

To overcome this problem, we sought to develop an alternative method of intracellular delivery that combines the microinjection concept with emerging tools from nanotechnology. We envisioned a "nanoinjector" that would penetrate cell membranes with minimal perturbation, delivering cargo to the cell's interior with high spatial resolution (at the nanometer scale). The proposed technology comprised three essential components: a needle with nanoscale diameter, a manipulator with nanoscale resolution, and controllable loading and releasing of cargo. Here we report the construction and successful operation of a cell nanoinjector in which a single multi-walled carbon nanotube (MWNT) attached to an atomic force microscope (AFM) tip served as the "nanoneedle" and an AFM integrated with an inverted fluorescence microscope served as the nanomanipulator (Fig. 1).

Results and discussion:

With needle-like geometry, large Young's modulus and high tensile strength (2, 3), carbon nanotubes (CNTs) are ideal nanoscale needles for this purpose. Their diameters can be selected from a range of 1-20 nm, a scale that allows physical penetration of a cell's membrane without significant disruption of the cell's macrostructure. Indeed, such a piercing, which is on the scale of a single protein's diameter, should readily heal by lipid diffusion without

perturbation of the cytoskeleton (4). Already, CNTs have demonstrated utility as cell transfection reagents and membrane penetrating delivery vehicles (5-8).

The nanomanipulation system was based on a commercially available AFM (MFP-3D-BIO^{TM}, Asylum Research, Santa Barbara, CA) that integrates an inverted fluorescence microscope (Nikon Eclipse TE2000-U). The AFM platform was ideal for this application, as it offers control of nanoneedle displacement at nanometer scale resolution and the ability to apply and monitor forces on the cell membrane. Thus, the AFM enabled precise positioning of the nanoneedle and high sensitivity monitoring of the membrane-piercing event.

The MWNT-AFM tips used in this work were fabricated as described previously (9). In brief, an individual MWNT of 10-20 nm in diameter was retrieved from a metal foil by the AFM tip using a nanomanipulator inside a scanning electron microscope (SEM). The MWNT was then cut to the desired length (0.5-1.5 μm) using an electron beam or electrical current. SEM and transmission electron microscopy (TEM) images of one representative MWNT-AFM tip are shown in Figures 2A and B, respectively.

For the controlled loading and release of cargo, we aimed to design a system that would obviate the need for a carrier solvent and, accordingly, the addition of excess volume to the cell's cytosol during the injection process. Toward this end, we exploited established chemical methods for CNT surface modification (10) and the intrinsic difference in redox potential between the intracellular and extracellular environments (11). Compound **1** (Fig. 3) fulfilled the functions of cargo loading and release as follows. Its pyrene moiety binds strongly to CNT surfaces via π-π stacking (12). Compound **1** is also endowed with a biotin moiety, separated from the pyrene group via a disulfide bond. In the relatively oxidizing environment of the cell's

exterior, the disulfide is stable. However, once exposed to the reducing environment of the cytosol, the disulfide is cleaved, liberating attached cargo.

To demonstrate the function of the nanoinjector, we sought to deliver quantum dots to the cell's cytosol without concomitant membrane and cell damage, effects that are hard to avoid with conventional delivery technologies (1). Quantum dots have emerged as powerful optical probes for single particle and single molecule studies in cellular systems (13). Their bright fluorescence and resistance to photobleaching have enabled single-particle tracking of membrane proteins on the cell surface (14) and vesicles within cells (15). Without a delivery vehicle, quantum dots cannot access the cell's cytosol and nuclei. Accordingly, processes therein have been refractory to study using quantum dot technology.

We coated the MWNT-AFM tip with compound **1** by co-incubation in methanol. The tip was then loaded with streptavidin-coated quantum dots (QDot® Streptavidin, Invitrogen) via non-covalent complexation of streptavidin with biotin in borate buffer (Fig. 3A). The loaded MWNT-AFM tips were characterized by TEM. As shown in Fig. 2C, multiple QDot® Streptavidin conjugates were successfully loaded onto a single MWNT functionalized with compound **1** (up to several hundred per 1-μM tip). In a control experiment, MWNT-AFM tips were incubated directly with QDot® Streptavidin without prior coating with compound **1**. In this case, no QDot® Streptavidin conjugates were observed on the MWNT surface (see Fig. 5, which is published as supporting information on the PNAS web site).

The nanoinjection experiments were then carried out using cultured HeLa cells, a human cervical epithelial cancer cell line. A target cell within the field of the optical microscope was identified, as indicated by the arrow in Figure 4B. The cantilever was then positioned on top of the target cell and the scan size was set to 0 nm. The deflection of the cantilever was measured

with a photodiode to monitor the displacement of the nanoneedle as the MWNT-AFM tip approached the cell surface. After the MWNT came into contact with the cell, the cantilever was further lowered so that the MWNT nanoneedle penetrated the membrane and reductive cleavage of disufide bonds allowed the release of QDot® Streptavidin conjugates within the cell. Following injection, the cantilever was retracted and the cell was imaged by fluorescence microscopy.

As shown in Fig. 4, fluorescence intensity inside the target cell indicated the release of quantum dots. QDot® Streptavidin conjugates were never observed in neighboring cells. We confirmed that the released quantum dots were within the cell's interior by video microscopy analysis. Their mobility was limited to the confines of the cell, where they exhibited slow diffusion and eventual immobilization, perhaps due to interactions with organelle membranes or cytoskeletal fibers (see Video 1, which is published as supporting information on the PNAS web site). Based on fluorescence intensity calibration experiments using free quantum dots in solution, and the sensitivity of our fluorescence microscope, we estimate that the fluorescence intensity in Fig. 4 represents small clusters of quantum dots with a diameter of 50-100 nm (i.e., 5-50 quantum dots depending on their arrangement).

To rule out the possibility that release of the QDot® Streptavidin conjugates occurred by desorption of the pyrene moiety from the MWNT surface rather than disulfide cleavage, we loaded cargo onto the MWNTs using control compound **2** (Fig. 3B). This linker possesses pyrene and biotin moieties, but replaces the disulfide bond with a polyethylene glycol (PEG) spacer separating the MWNT and streptavidin binding elements. We functionalized MWNT-AFM tips with **2** and then loaded QDot® Streptavidin conjugates onto the nanoneedle. The modified MWNT-AFM tips were analyzed by TEM and were similar to MWNT-AFM tips

bearing the disulfide-bound conjugates (see Fig. 6, which is published as supporting information on the PNAS web site). Similar nanoinjection experiments were carried out using HeLa cells but in this case no QDot® Streptavidin conjugates were released (with >5 different MWNT-AFM tips in >10 injection experiments) (see Fig. 7, which is published as supporting information on the PNAS web site). These results have two important implications. First, the release mechanism is dependent on disulfide bond cleavage and is therefore not simply due to desorption of the pyrene moiety from the MWNT surface. Second, the requirement of disulfide cleavage confirms that cargo release occurred within the reducing environment of the cytosol.

A limitation of many intracellular delivery technologies is the harmful effects they exert on membranes and cells. Therefore, we probed the effects of nanoinjection on membrane integrity and cell viability using three assays: (i) the trypan blue exclusion assay (16), (ii) the Calcein AM assay (17), and (iii) the Annexin V-FITC/propidium iodide (PI) assay for apoptosis (18) (experimental details are in the Supporting Information). In the trypan blue assay, the dye was added immediately after cell nanoinjection and the cells were monitored for10 hours thereafter. No trypan blue inclusion or reduction in cell viability was observed during this time period (see Table 1, which is published as supporting information on the PNAS web site). In the Calcein AM assay, the cells were loaded with the fluorescent dye immiately prior to nanoinjection. Similar to the previous results, we saw no evidence of compromised membrane integrity for up to 10 hours (see Fig. 8, which is published as supporting information on the PNAS web site). Finally, nanoinjected cells showed no detectable staining with Annexin V-FITC or PI up to 10 hours after the event (see Fig. 9, which is published as supporting information on the PNAS web site). Thus, nanoinjection does not appear to induce apoptotic

pathways in the cells. Notably, the biocompatibility of nanoinjection should allow for exploration of a broad range of release chemistries that occur over extended time periods.

The ability to deliver quantum dots to the cell's cytoplasm provides a platform for numerous studies of intracellular processes. As an example, we used the single-particle tracking technique (14, 15, 19) to characterize the diffusion dynamics of injected quantum dots in the cytosol, which has been previously studied using methods that can harm cells (20). After nanoinjection, the diffusion dynamics of cytosolic quantum dots were characterized by analyzing the mean square distance (Δr^2) and traveling time (Δt) for an injected quantum dot cluster (see Fig. 10, which is published as supporting information on the PNAS web site). The slope of the best-fit line afforded a diffusion coefficient of 0.3 μm^2/sec. This value is approximately 10-fold lower than diffusion coefficients measured in pure water, which is consistent with previous measurements (20). A major advantage of the biocompatible nanoinjection technology is that the process can be performed repeatedly, or in tandem with other measurements, throughout the normal life cycle of the cell.

In summary, the nanoinjector provides a fundamentally new mechanism for delivering a discrete, small number of molecules into cells without need for carrier solvent and with no apparent cell damage. The unique capabilities of the nanoinjector can be further exploited in a number of ways. Other biomolecules such as DNA and RNA, or synthetic structures such as polymers, dendrimers and nanoparticles can be delivered into cells in a similar fashion. In conjunction with organelle-specific optical probes, the nanoinjector concept might be extended to the delivery of cargo to specific subcellular compartments. In principle, cells such as bacteria that are too small for microinjection should be amenable to nanoinjection. Notably, the

architecture of the nanoinjector allows the use of AFM to identify a target cell and position the nanoneedle, and is therefore not limited by the resolution of light microscopy.

Materials and Methods:

Materials. All chemical reagents were of analytical grade, obtained from commercial suppliers and used without further purification. The synthetic procedure of compound **1** and **2** is described in detail in supporting information published on the PNAS web site.

Fabrication of MWNT-AFM tips The fabrication of MWNT-AFM tips was carried out in an FEI Sirion XL 30 SEM, equipped with a home-made manipulator. The procedure was described in detail in a previous publication (9).

SEM and TEM characterization. SEM images of MWNT-AFM tips were obtained on an FEI Sirion XL 30 SEM operated at 5 keV. TEM images of unfunctionalized and functionalized MWNT-AFM tips were obtained on a JEOL 2011 microscope operating at an electron energy of 100 keV. A home-made holder was used for loading MWNT-AFM tips.

Functionaliztion of MWNT-AFM tips. QDot® 655 Streptavidin conjugates (1 μM solution, purchased from Invetrogen) were centrifuged at 5,000 × g, reserving the supernatant, prior to use. The MWNT-AFM tips were incubated with linker **1** or **2** (1 μM, MeOH) at rt for 1 h, followed by washing 3 times with methanol and borate buffer (50 mM, pH = 8.3), respectively. The MWNT-AFM tips functionalized with **1** or **2** were then incubated with blocking buffer (borate buffer containing 1% BSA) for 30 min. The blocked MWNT-AFM tips were then transferred to a solution of QDot® 655 Streptavidin conjugates (1:25 dilution) in borate buffer and incubated at rt for 30 min, followed by washing with borate buffer for 3 times. The functionalized MWNT-AFM tips were then used directly for nanoinjection experiments or dried

under N_2 for TEM characterization. In a control experiment, the MWNT-AFM tips were incubated with blocking buffer for 30 min. The blocked MWNT-AFM tips were then transferred to a solution of QDot® 655 Streptavidin conjugates (1:25 dilution) in borate buffer and incubated at rt for 30 min, followed by washing 3 times with borate buffer. The MWNT-AFM tips were then dried under N_2 for TEM characterization.

Cell culture conditions. HeLa cells were grown in DMEM supplemented with penicillin (100 unit/mL), streptomycin (0.1 mg/mL), and 10% FCS and maintained in a 5% CO_2, water-saturated atmosphere at 37 ^{o}C.

Cell Viability Studies. The Hela cells after nanoinjection were studied using three cell viability assays: trypan blue exclusion assay, Calcein AM assay, and Annexin V-FITC/propidium iodide assay. The experimental procedure is described in detail in supporting information published on the PNAS web site.

Acknodgements:

We thank C. Bustamante and J. Martinez for help on developing MWNT-AFM tips, U. C. Tam for assistance with cell culture experiments, K. Zhang for assistance with data analysis, G. S. Rangan for assistance with graphics, M. Paulick, R. Chandra, P. Wu, and W. Michelson for helpful discussions, and L. Sohn and R. Dylla-Spears for sharing the instruments. This work was supported by the Director, Office of Energy Research, Office of Basic Energy Sciences, Division of Materials Sciences, of the U. S. Department of Energy under Contract No. DE-AC03-76SF00098, within the Interfacing Nanostructures Initiative, and by the National Science Foundation via the Center of Integrated Nanomechanical Systems. Portions of this work were performed at the Molecular Foundry, Lawrence Berkeley National Laboratory, which is supported by the Office of Science, Office of Basic Energy Sciences, of the U.S. Department of Energy under Contract No. DE-AC02--05CH11231.

References:

1. Stephens, D. J. & Pepperkok, R. (2001) *Proc. Natl. Acad. Sci. USA* **98,** 4295-4298.
2. Yu, M. F., Files, B. S., Arepalli, S. & Ruoff, R. S. (2000) *Phys. Rev. Lett.* **84,** 5552-5555.
3. Yu, M. F., Lourie, O., Dyer, M. J., Moloni, K., Kelly, T. F. & Ruoff, R. S. (2000) *Science* **287,** 637-640.
4. Vereb, G., Szollosi, J., Matko, J., Nagy, P., Farkas, T., Vigh, L., Matyus, L., Waldmann, T. A. & Damjanovich, S. (2003) *Proc. Natl. Acad. Sci. USA* **100,** 8053-8058.
5. Pantarotto, D., Singh, R., McCarthy, D., Erhardt, M., Briand, J. P., Prato, M., Kostarelos, K. & Bianco, A. (2004) *Angew. Chem. Int. Ed* **43,** 5242-5246.
6. Cai, D., Mataraza, J. M., Qin, Z. H., Huang, Z. P., Huang, J. Y., Chiles, T. C., Carnahan, D., Kempa, K. & Ren, Z. F. (2005) *Nat. Methods* **2,** 449-454.
7. Kam, N. W. S., O'Connell, M., Wisdom, J. A. & Dai, H. J. (2005) *Proc. Natl. Acad. Sci. USA* **102,** 11600-11605.
8. Kouklin, N. a., Kim, W. E., Lazareck, A. D. & Xu, J. M. (2005) *Appl. Phys. Lett.* **87,** 173901-173903.
9. Martinez, J., Yuzvinsky, T. D., Fennimore, A. M., Zettl, A., Garcia, R. & Bustamante, C. (2005) *Nanotechnology* **16,** 2493-2496.
10. Lin, Y., Taylor, S., Li, H. P., Fernando, K. A. S., Qu, L. W., Wang, W., Gu, L. R., Zhou, B. & Sun, Y. P. (2004) *J. Mat. Chem.* **14,** 527-541.
11. Saito, G., Swanson, J. A. & Lee, K. D. (2003) *Adv. Drug Deliv. Rev.* **55,** 199-215.
12. Chen, R. J., Zhang, Y., Wang, D. & Dai, H. (2001) *J. Am. Chem. Soc.* **123,** 3838-3839.
13. Michalet, X., Pinaud, F. F., Bentolila, L. A., Tsay, J. M., Doose, S., Li, J. J., Sundaresan, G., Wu, A. M., Gambhir, S. S. & Weiss, S. (2005) *Science* **307,** 538-544.
14. Dahan, M., Levi, S., Luccardini, C., Rostaing, P., Riveau, B. & Triller, A. (2003) *Science* **302,** 442-5.
15. Nan, X. L., Sims, P. A., Chen, P. & Xie, X. S. (2005) *J. Phys. Chem. B* **109,** 24220-24224.
16. Arrigo, A. P., Firdaus, W. J. J., Mellier, G., Moulin, M., Paul, C., Diaz-latoud, C. & Kretz-remy, C. (2005) *Methods* **35,** 126-138.
17. Bratosin, D., Mitrofan, L., Palii, C., Estaquier, J. & Montreuil, J. (2005) *Cytometry A* **66,** 78-84.
18. Moore, A., Donahue, C. J., Bauer, K. D. & Mather, J. P. (1998) *Methods Cell Biol.* **57,** 265-78.
19. Babcock, H. P., Chen, C. & Zhuang, X. W. (2004) *Biophys. J.* **87,** 2749-2758.
20. Luby-Phelps, K. (2000) *Int. Rev. Cytol.* **192,** 189-221.

Figure Lengends:

Fig. 1. Schematic of the nanoinjection procedure: A MWNT-AFM tip with cargo attached to the MWNT surface via a disulfide linker penetrates a cell membrane. After disulfide reduction within the cell's cytosol, the cargo is released and the nanoneedle is retracted.

Fig. 2. (A) SEM image of a MWNT-AFM tip. **(B)** TEM image of the tip region of **(A)**. **(C)** TEM image of a MWNT-AFM tip coated with linker **1** and conjugated with QDot® Streptavidin.

Fig. 3. Functionalization of MWNT-AFM tips. **(A)** QDot® Streptavidin was attached to the MWNT surface though linker **1** containing a disulfide bond: (i) **1**, MeOH; (ii) QDot® Streptavidin, borate buffer. **(B)** QDot® Streptavidin was attached to the MWNT surface though linker **2** containing no disulfide bond: (iii) **2**, MeOH; (iv) QDot® Streptavidin, borate buffer.

Fig. 4. Nanoinjection of QDot® Streptavidin conjugates into a target HeLa cell. **(A)** Fluorescence image of the cells before nanoinjection. **(B)** Combined bright-field and fluorescence image of the cells before nanoinjection. The inserted arrow indicates the target cell. The dark shape in the lower left corner is the AFM cantilever. **(C)** Fluorescence image of the cells after the nanoinjection, showing fluorecent QDot® Streptavidin conjugates released inside the target cell. **(D)** Combined bright-field and fluorescence image of the cells after the nanoinjection. The QDot® Streptavidin conjugates are shown in red. The dark shape in the upper left corner is the retracted AFM cantilever. (**E**) Combined bright-field and fluorescence image of another four examples of HeLa cells after nanoinjection of QDot® Streptavidin. In all cases, fluorescence images were acquired with λ_{ex} = 415 nm and data collection with a 655 nm filter. Images are 70 × 70 μm in (A)–(D) and 30 × 30 μm in (E).
Fig. 1.

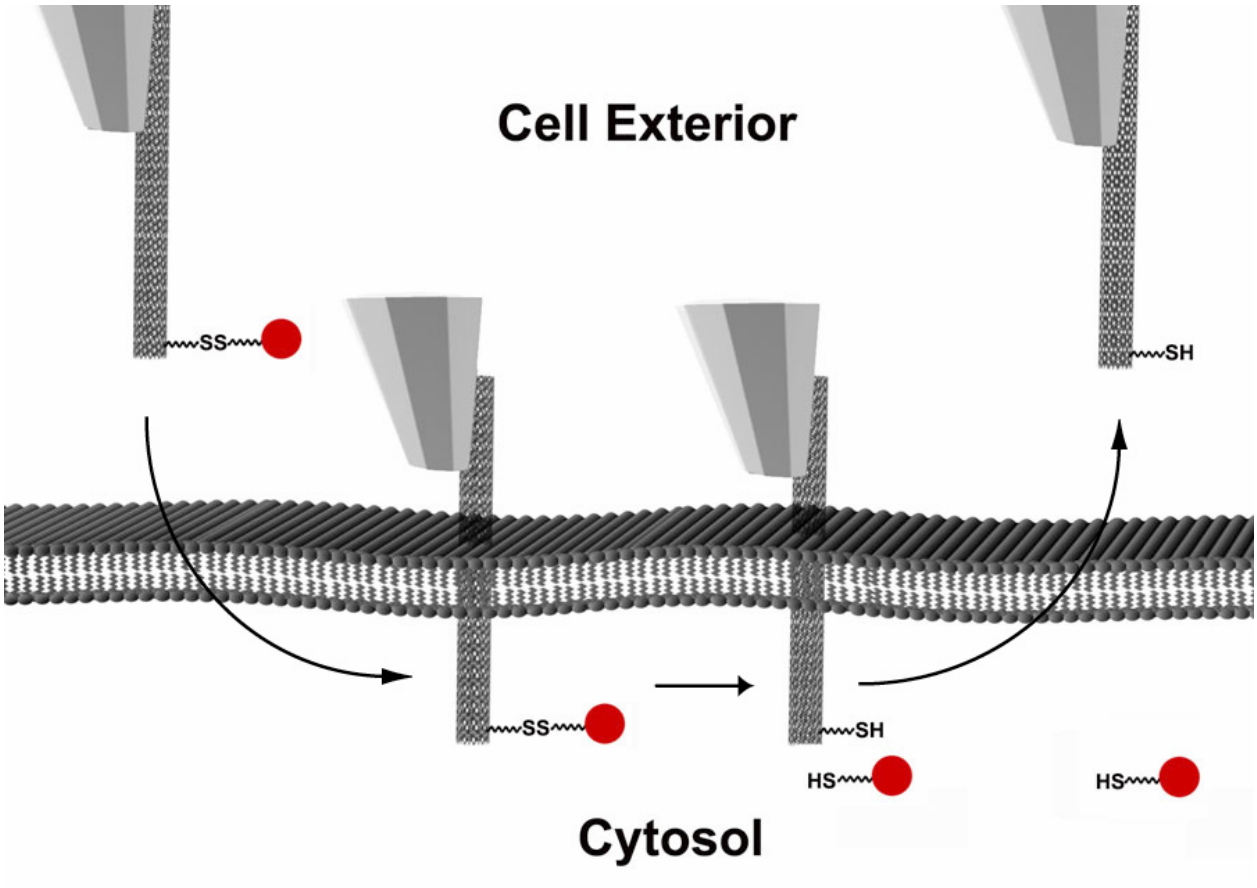
Cell Exterior
SS
SH
SS
SH
HS
HS
Cytosol

Fig. 2.

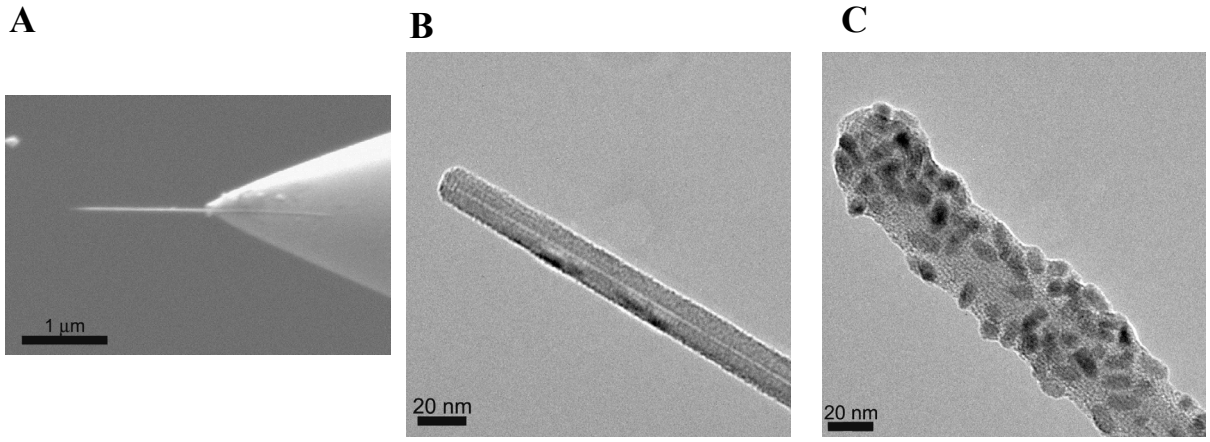

Fig. 3.

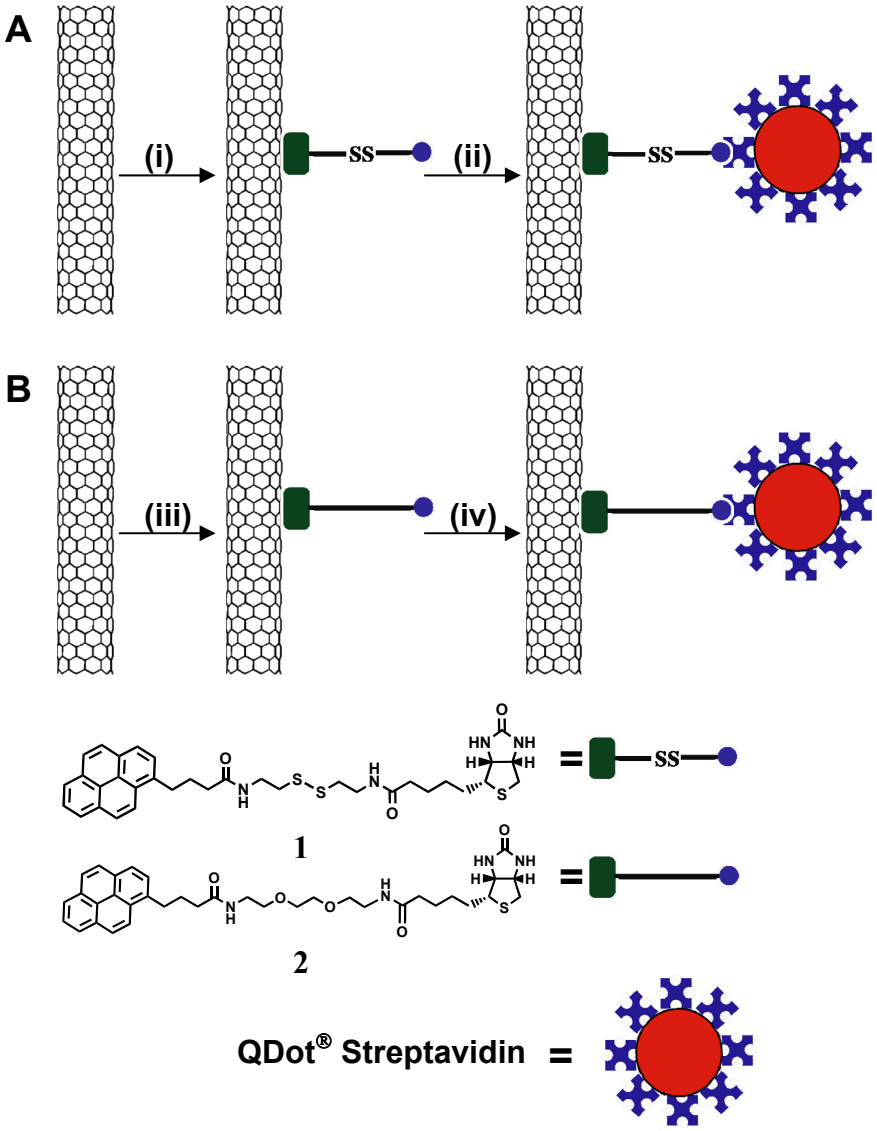

Fig. 4.